Onset of spin-density-wave antiferromagnetism in Cr/V multilayers

E. Kravtsov,[1,2,*] R. Brucas,[3] B. Hjörvarsson,[3] A. Hoser,[4,5,†] A. Liebig,[3] G. J. McIntyre,[6] M. A. Milyaev,[2] A. Nefedov,[1] L. Paolasini,[7] F. Radu,[1,‡] A. Remhof,[1,§] V. V. Ustinov,[2] F. Yakhou,[7] and H. Zabel[1]

[1]*Institut für Experimentalphysik/Festkörperphysik, Ruhr-Universität Bochum, D-44780 Bochum, Germany*

[2]*Institute of Metal Physics, 620219 Ekaterinburg, Russia*

[3]*Department of Physics, Uppsala University, SE-75121 Uppsala, Sweden*

[4]*Institut für Kristallographie, RWTH-Aachen, D-52056 Aachen, Germany*

[5]*Institut für Festkörperforschung, Forschungszentrum Jülich, D-52425 Jülich, Germany*

[6]*Institut Laue-Langevin, F-38042 Grenoble, France*

[7]*European Synchrotron Radiation Facility, F-38043 Grenoble, France*

(Received 25 March 2007; published 17 July 2007)

Spin-density-wave (SDW) magnetism in a series of Cr/V heterostructures with different Cr thicknesses was systematically investigated by combined resistivity, neutron, and synchrotron scattering measurements. We show that the onset of the bulklike SDW state comes through several necessary steps from a paramagnetic state through a commensurate SDW to an incommensurate SDW. The Néel temperature for the incommensurate SDW is found to scale with Cr thickness and reaches the bulk value at a Cr thickness of about 2000 Å. The proximity effect from Cr/V interfaces is found to lead to (i) the appearance of a 50-Å magnetically dead Cr layer near Cr/V interfaces and (ii) suppression of the spin-flip transition and stabilization of a single-domain SDW with out-of-plane spins and out-of-plane propagation wave vector. Finally, we show that the SDW period increases with decreasing Cr thickness and becomes temperature independent in sufficiently thin Cr layers.

DOI: 10.1103/PhysRevB.76.024421 PACS number(s): 75.70.Ak, 61.12.Ld, 75.30.Fv

I. INTRODUCTION

The itinerant antiferromagnetism in Cr has attracted considerable attention during the last 40 years.[1] Its low-temperature behavior is associated with the existence of spin-density waves (SDWs) incommensurate with the bcc lattice periodicity of Cr, with the Néel temperature T_N being about 311 K for bulk Cr. The incommensurate spin-density wave (ISDW) consists of a sinusoidal modulation of the amplitude of the antiferromagnetically ordered Cr magnetic moments. At the spin-flip transition temperature of 123 K, the SDW polarization changes from longitudinal (LSDW) with magnetic moments aligned parallel to the wave propagation direction to transverse (TSDW), where the magnetic moments align perpendicular to the wave propagation direction. The SDW in Cr-based systems coexists with a charge-density wave (CDW) and a strain wave (SW) corresponding to periodic modulations of the charge density and the lattice spacing, respectively, with half the period of the SDW. Elastic strains, defects, and chemical impurities in bulk Cr systems may cause the SDW to be commensurate (CSDW) with the Cr lattice periodicity. In this case there is no modulation in the value of Cr magnetic moments and the system looks like a simple antiferromagnet. The CSDW phase is often reported to be stable at temperatures much higher than the Néel temperature of the incommensurate phase.

Whereas the SDW behavior in bulk Cr and Cr-based alloys is well established now,[1,2] there are a good number of gaps in our understanding of its nature in Cr thin films and heterostructures.[3] In bulk Cr the SDW properties are connected with peculiar features of the Cr Fermi surface, which provide nesting vectors between electron and hole sheets of similar shape.[1,4] In thin Cr-based heterostructures, the SDW is confined and therefore spontaneous formation of the SDW due to Fermi-surface nesting competes with hybridization and exchange-coupling effects of adjacent layers, with interfacial structures (order and disorder), with additional epitaxial strains due to lattice misfits, and with dimensionality effects (film thickness dependence). As the Cr film becomes thicker, these competitive effects become weaker and finally one approaches a bulklike spontaneous ISDW state. The onset of bulklike SDW order in Cr-based heterostructures as the Cr film increases in thickness is still unexplored terrain in the SDW magnetism. What the roles of epitaxial strain and boundary conditions are on the onset of magnetism in thin Cr films, how global SDW properties (Néel temperature, ISDW period, magnetic phase diagram) depend on Cr thickness, and whether there is a crossover between commensurate and incommensurate phases are key issues for understanding SDW physics.

Today, a substantial body of literature has evolved which traces different aspects of the SDW magnetism in Cr-based heterostructures, but it is very difficult to draw a uniform picture due to the very complex physics in these systems and potential artifacts. Experimental results provided by different groups are difficult to merge because they were obtained with samples grown under different experimental conditions in different laboratories. Fe/Cr multilayer structures have received the most interest (see, for example, the reviews in Refs. 3–5 and references therein). It was found that, when growing on a flat (001)Fe surface, Cr becomes magnetic from the very first monolayer and forms a CSDW.[6,7] At some critical thickness the SDW switches to the incommensurate phase. Neutron scattering and resistivity measurements on (001)Fe/Cr multilayers[8–10] have shown that the Néel temperature for the incommensurate phase scales with Cr thickness and it is suppressed when Cr layers become thinner than some critical thickness near 50 Å. The incommensurate

SDW propagates normal to the film surface and has a transverse polarization with in-plane spins.[10,11] No systematic information is presently available about the SDW evolution with thickness in other Cr-based systems. We do not know if the above findings are unique to Fe/Cr multilayers or if they are common to a wide class of Cr-based heterostructures.

Here we address Cr/V-multilayered systems, which also promise rich physics but have been much less studied so far. The main effects in these systems do not originate from interface exchange interactions as in Fe/Cr but from the hybridization between the very similar Fermi surfaces of Cr and V, epitaxial strains, and finite-size effects. Studies of bulk CrV alloys[12–15] have revealed a quick suppression of the SDW state with V concentration, including a decrease in both the Cr magnetic moment and the Néel temperature. The effect was found to be so strong that a concentration of only 4 at. % V is enough to suppress totally the SDW state in CrV alloy.

It was theoretically predicted[16] that the Cr-V interface hybridization would cause a short-range suppression of the SDW magnetism near Cr/V interfaces, which may be considered as pinning of SDW nodes at the interfaces. Almokhtar and co-workers[17,18] have provided experimental evidence for a strong suppression of Cr magnetic moments near Cr/V interfaces. They have conducted a series of elegant experiments with Mössbauer spectroscopy by inserting ^{119}Sn probe layers into Cr/V multilayers at different distances from the interfaces. They have found Cr to be nonmagnetic at distances up to 10–20 Å away from the interface, while at larger distances of about 20 Å the Cr magnetic moments increase again and reach values comparable to the bulk moment.

While the effect was expected to be of local nature and should have vanished at distances of about 20 Å from the Cr/V interface, we have recently shown[19,20] that it nevertheless produces a global perturbation of the SDW magnetism in rather thick Cr films, including changes in the SDW polarization and propagation direction. In the present article we report on our investigations of Cr/V magnetism performed with a series of Cr/V heterostructures grown with different Cr thicknesses in the range from 90 to 2000 Å. The samples were grown under the same conditions and their structural properties were carefully characterized, providing comprehensive information about the crystalline structure and the epitaxial strains. From combined resistivity, neutron, and synchrotron scattering experiments we draw a systematic picture of the SDW evolution in Cr/V heterostructures with Cr thickness. We trace the onset of the Cr magnetism in thin-film systems and its further modification with Cr thickness towards a bulklike SDW state. The influence of finite-size and proximity effects on the Néel temperature, SDW period, and magnetic phase diagram of Cr/V heterostructures is analyzed in detail.

II. SAMPLE GROWTH AND STRUCTURAL CHARACTERIZATION

The investigations were done on a series of $[\mathrm{Cr}(t_{cr})/\mathrm{V}(14\ \text{Å})]_N$ multilayers grown with a UHV sputtering machine onto MgO(001) substrates. During the growth we have deposited first a V buffer layer of 14 Å thickness and continued with a Cr/V multilayered film. The V thickness was held constant at 14 Å for each sample, and the Cr thickness t_{Cr} was varied from 90 Å to 2000 Å. The number of repetitions, N, was 23 for the Cr(90 Å)/V sample, whereas for those with t_{Cr}=125, 250, 500, 1000, and 2000 Å it was adjusted such that the total Cr thickness in the samples was equal to 2000 Å. The samples were capped with a 30-Å-thick Pd layer to protect them from oxidation. During the deposition of the samples the substrate temperature was kept at 200 °C.

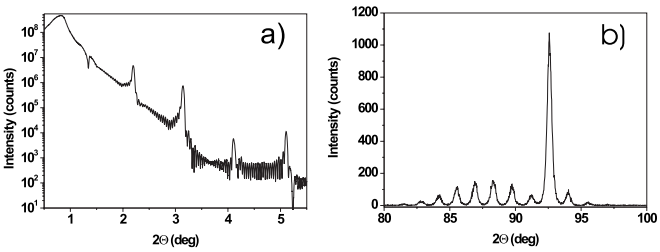

FIG. 1. (a) Reflectivity profile from a $[\mathrm{Cr}(90\ \text{Å})/\mathrm{V}(14\ \text{Å})]_{23}$ multilayer at a wavelength λ=2.084 Å, indicating a good layering throughout the multilayer. (b) Wide-angle x-ray diffraction pattern taken from the same multilayer through the fundamental Cr/V(002) Bragg position. The Cr/V(002) peak and its multiple satellite reflections indicate a very high quality of the crystalline structure.

Structural properties of the samples were characterized with x-ray scattering methods including reflectometry, wide-angle, and grazing incidence diffraction. The x-ray measurements were done at the W1.1 beamline of HASYLAB (Hamburg, Germany) and the SAW beamline of DELTA (Dortmund, Germany). The x-ray measurements were performed at room temperature using wavelengths of 2.084 Å, 1.540 Å, and 0.94 Å.

Individual layers thicknesses and interface structure were determined from x-ray reflectometry measurements. In Fig. 1(a) is shown a reflectivity profile from the $[\mathrm{Cr}(90\ \text{Å})/\mathrm{V}(14\ \text{Å})]_{23}$ multilayer measured at a wavelength of 2.084 Å. Pronounced superlattice reflections and short-period oscillations from the total multilayer thickness observed in the profile are indications of a good layering throughout the multilayer, smooth film surface, and well-defined interfaces. The Cr/V(001) epitaxial growth was confirmed by wide-angle x-ray diffraction measurements. In Fig. 1(b) is shown a $\Theta-2\Theta$ scan taken for the same sample through the Cr/V(002) Bragg reflection. Multiple satellite reflections observed in the diffraction pattern indicate a high quality of the crystalline structure. The in-plane structure and epitaxial relations were determined by surface x-ray diffraction. The epitaxial relation between Cr/V and MgO for all the series was found to be Cr(001)[100]$\|$MgO(001)[110], which is in agreement with reports for growth of Cr directly on the MgO(001) substrate.[21]

In Table I we summarize structural parameters of the Cr/V heterostructures as deduced from an analysis of x-ray scans taken around the out-of-plane (002) and in-plane (110) fundamental Cr/V Bragg reflections. The Cr out-of-plane lattice parameter $a_\perp$ and crystal coherence length $\xi_\perp$ were

TABLE I. Lattice parameters, crystal coherence lengths, and mosaic spreads in Cr/V heterostructures on MgO(001) substrates. The thickness of every V layer in all samples is 14 Å.

Sample	$a_\perp$ [Å]	$a_\parallel$ [Å]	$\xi_\perp$ [Å]	$\xi_\parallel$ [Å]	Mosaicity [deg]
V/Cr(2000 Å)/V	2.892	2.923	2000	500	0.10
$[Cr(1000\ Å)/V]_2$, phase I (95%)	2.889	2.903	400	200	0.36
$[Cr(1000\ Å)/V]_2$, phase II (5%)	2.889	2.972	400	200	0.36
$[Cr(500\ Å)/V]_4$	2.886	2.897	300	400	0.41
$[Cr(250\ Å)/V]_8$	2.882	2.895	100	100	0.70
$[Cr(125\ Å)/V]_{16}$	2.875	2.897	100	100	0.65
$[Cr(90\ Å)/V]_{23}$	2.883	2.895	100	100	0.44

determined from the position and width of the fundamental Cr/V (002) Bragg reflections in Θ-2Θ geometry. The in-plane mosaic spread was estimated from rocking θ scans taken through the same reflections. The in-plane lattice parameter $a_\parallel$ and crystal coherence length $\xi_\parallel$ were estimated from grazing-incidence diffraction scans taken through the in-plane (110) Bragg reflections, the incidence angle of the beam being fixed at a value corresponding to x-ray penetration into the upper Cr layer to a depth of about 50 Å.

As follows from the data in the Table I, the in-plane lattice parameters of all samples are expanded as compared to the bulk value a_{Cr}=2.884 Å. This is very likely to be due to an in-plane epitaxial tensile stress from the MgO(001) substrate and the V layers, which have larger bulk in-plane lattice parameters (a_V=3.03 Å, $a_{MgO}/\sqrt{2}$=2.978 Å). The first sample of the series Cr(2000 Å)/V features an extremely high degree of structural correlation. Its out-of-plane structural correlation length is about 2000 Å, which corresponds exactly to the total Cr layer thickness. We speculate that its structural correlation with the substrate and adjacent V layers is also very high. Its lattice is significantly expanded both in plane and out of plane, so this sample undergoes the maximum epitaxial strains. As the Cr layer thickness decreases and the number of V interlayers increases, the structure integrity decreases, which manifests in shorter structural correlation lengths and larger in-plane mosaic. The lattice parameters decrease, approaching that of the corresponding Cr bulk value, and thus the epitaxial strain in these samples also decreases.

For the Cr(1000 Å)/V sample we observed two phases characterized by different in-plane lattice parameters $a_\parallel$. As estimated from the integral intensities of the (110) Bragg peaks, the first phase occupies about 95% of the sample, the rest of the sample being occupied by the second phase. It is not possible to estimate exactly the ratio of these two phases throughout the sample because in our in-plane measurements we do not probe the sample totally but only its upper part. The in-plane lattice parameter for the second phase appears to be rather close to that of MgO. Nevertheless, the second phase with the larger $a_\parallel$ is clearly seen and, as we will show below, it plays its part in forming the SDW state in this sample.

III. RESISTIVITY MEASUREMENTS OF THE NÉEL TEMPERATURE

The Néel temperature T_N of the incommensurate SDW phase in the samples was estimated from resistivity measurements. Transport properties were measured using a standard four-terminal dc technique in a PPMS device (Quantum Design). The measurements were taken at temperatures from 2 to 340 K with a magnetic field of 1 kOe applied in the film plane. This technique is well established now and has been successfully applied to identify T_N in bulk Cr,[1] Cr alloys,[2] thin Cr films,[8] and Cr-based superlattices.[9]

The method is based on the fact that the resistivity ρ is enhanced as the temperature T decreases through T_N and the paramagnetic Cr state changes to the SDW one. As an example of typical resistivity anomalies, in Fig. 2 are shown the results of resistivity measurements for the Cr(2000 Å)/V(14 Å) sample. The Néel transitions manifest themselves as a sharp minimum in the $d\rho/dT$ curve. As will be seen below, the T_N for this sample corresponds to the transition from an SDW to a paramagnetic state. For the rest of the samples the resistivity anomaly is not so pronounced, probably because there occurs a transition from an incommensurate to commensurate SDW state, which may not be so sharp. No resistivity anomaly was observed for the samples with Cr thickness of 90 and 125 Å.

IV. SCATTERING EXPERIMENTS

The SDW properties of Cr/V heterostructures were determined by combined neutron and x-ray scattering experiments. Magnetic scattering of neutrons is directly sensitive to the magnetic state of Cr and, in principle, it is able to provide very complete information on the SDW state in Cr films. The

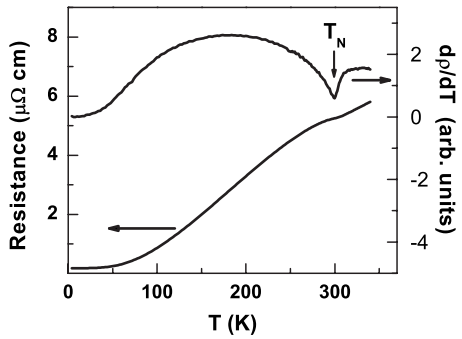

FIG. 2. Resistance measurements on the Cr(2000 Å)/V(14 Å) sample to locate the Néel temperature defined as the minimum in the $d\rho/dT$ curve.

Cr magnetic moment modulation produces corresponding satellite reflections in the vicinity of forbidden Cr bcc Bragg reflections, which can be detected with neutron scattering. In the case of a commensurate SDW the neutron scattering reflections will be detected exactly at forbidden Bragg peaks. The position and intensity of these satellite reflections contain information on the Cr spin orientation as well as on the amplitude, period, and propagation direction of the spin-density waves. However, neutron scattering requires a significant amount of scattering material. In our case, due to thin films, the intensity of the detected satellite reflections is often rather low and we cannot reach a good resolution in Q space because of poor statistics. For the precise determination of the period and Néel temperature of incommensurate SDWs we performed x-ray scattering experiments by detecting satellite reflections arising around fundamental Cr Bragg peaks due to strain waves. Although SW investigations do not reveal the SDW polarization, they have the advantage of a higher reciprocal-space resolution. In our analysis we used neutron scattering results for a qualitative description of the SDW behavior (magnetic phase diagram) and x-ray data to gain quantitative results. The application of neutron and x-ray scattering methods to the determination of the SDW parameters has been well described in the literature, and we refer to published works and reviews for further information.[1,3,22,23] The neutron and x-ray cross sections and selection rules for different cases of SDW polarizations and propagation directions can also be found in the above-cited papers.

The neutron scattering experiments were performed at the triple-axis spectrometer UNIDAS (Forschungszentrum Jülich, Germany) and the four-circle diffractometer D10 (Institut Laue-Langevin, Grenoble, France). In the experiments we used pyrolytic graphite (PG) monochromators to select a neutron beam wavelength of $\lambda = 2.351$ Å together with PG transmission filters to reduce the $\lambda/2$ monochromator contamination. The background radiation was sufficiently filtered out by using PG analyzer crystals fixed to zero energy transfer. The measurements were taken at temperatures between 10 and 330 K by using a Displex cryostat (UNIDAS) or a He-flow cryostat (D10) with Al windows.

The strain-wave properties in the Cr/V heterostructures were determined by synchrotron scattering experiments at the ID20 magnetic scattering undulator beamline of the ESRF (Grenoble, France)[24]. The incident photon beam delivered by two phase undulators was 99.8% linearly σ polarized in the sample plane. The primary slits in the optical system were set to utilize the third harmonic of the undulators. The incident beam energy was selected to be 12 keV by using a PG double-crystal monochromator. The polarization of the scattered beam was analyzed by using a pyrolytic graphite PG(004) analyzer to select pure $\sigma\sigma$ scattered intensity, also providing a drastic reduction of the background signal. The x-ray measurements were taken at temperatures between 15 and 310 K by using a Displex cryostat equipped with Be windows.

V. SPIN-DENSITY WAVES IN Cr/V HETEROSTRUCTURES

In this section we present experimental data and summarize qualitative information on the SDW behavior in Cr/V heterostructures as revealed from our neutron and synchrotron experiments. As a rule, in our investigation we used neutron results to establish magnetic phase diagrams for SDWs in Cr/V systems, to determine SDW polarizations, and to distinguish commensurate and incommensurate SDW phases. Synchrotron results were used mainly for the precise determination of the ISDW period and Néel temperature, in the last case together with resistivity measurements.

In our x-ray measurements we always performed two screening scans: one scan at the Cr(101) fundamental Bragg reflection in the in-plane (H) direction to check for possible incommensurate SWs propagating in-plane and the other scan along the out-of-plane (L) direction, crossing the Cr(002) fundamental Bragg reflection to search for out-of-plane incommensurate SWs. These two scans are enough to determine the propagation direction of the SWs. As for neutron measurements, in each case we performed four scans across the (100) and (001) positions in the in-plane (H) and out-of-plane (L) directions. These four scans are enough to determine the polarization and propagation direction of the SDW's in our Cr/V heterostructures. Table II summarizes the selection rules for the appearance of magnetic commensurate and satellite reflections in these four scans.[22] Due to the large amount of experimental material, in the following we do not present all scans performed but show only important scans providing essential information on the SDW state. (If some scans are not shown in the article, this means that we have performed these scans but detected no signal.)

(i) V/Cr(2000 Å)/V *heterostructures*. In Fig. 3 are shown synchrotron radiation scans from the V/Cr(2000 Å)/V sample taken at different temperatures. The fundamental (002) and (101) Cr peaks are removed from the figures for clarity as their intensity is many orders of magnitude higher than the intensity of the satellite reflections. In the panel on the right-hand side, the scan directions are indicated. From the recorded scans it is evident that in our case the strain wave propagates entirely out of the film plane, whereas the in-plane wave is completely suppressed. As evident from the picture, the satellite positions move smoothly towards the (002) peak as temperature increases, while the intensity decreases continuously with temperature. The SW satellite on the low-L side of the Cr(002) reflection is less pronounced due to a significant contamination from the fundamental V(002) reflection. The satellite positions provide us the information about the SW period, which increases with temperature. The Néel temperature of the system is estimated to be about 270 K where the satellite peak intensity has vanished, which agrees with the resistivity data presented in Fig. 2.

The SDW polarization was determined by neutron diffraction measurements. In Fig. 4 are presented neutron diffraction scans performed in the L directions in the vicinity of the Cr(100) and Cr(001) positions in reciprocal space. On the right-hand side of each set the scan directions are indicated. As is evident from the scans, at low temperatures below 60 K we observe magnetic satellites only around the Cr(100) position and no intensity around the Cr(001) peak. From this we infer that in these temperatures only a longitudinal SDW exists. At 60 K and above we observe satellite reflections

TABLE II. Selection rules for the appearance of (1 0 0), (0 0 1) commensurate reflections and satellites due to longitudinal and transverse spin-density waves in Cr thin films and heterostructures. LSDW and TSDW refer to the propagation direction of the spin-density wave, parallel and perpendicular, respectively, to the Cr moments, while the horizontal and vertical arrows denote the direction of the Cr moments themselves, parallel and perpendicular, respectively, to the film surface. An × indicates that a peak should be present; blank entries indicate that a peak should not be present.

Reflection	In-plane LSDW →	Out-of-plane LSDW ↑	In-plane TSDW →	In-plane TSDW ↑	Out-of-plane TSDW →	CSDW →	CSDW ↑
1 0 0						×	×
$1\pm\delta$ 0 0			×	×			
1 0 $\pm\delta$		×			×		
0 0 1						×	
0 0 $1\pm\delta$					×		
$\pm\delta$ 0 1	×		×				

around both the Cr(100) and Cr(001) positions, which is an indication for a spin-flip transition from the longitudinal SDW to a transverse SDW both with propagation direction perpendicular to the film plane. No intensity was detected at the commensurate (100) and (100) positions, indicating that the SDW in this sample is completely incommensurate. The Néel temperature as estimated from the neutron data of Fig. 4 seems to be lower than 270 K as we know from the above synchrotron and resistivity results. We relate this disagreement to the fact that the neutron magnetic intensity is much lower compared to the synchrotron structural one, which makes x-ray data more reliable when working with thin Cr films close to T_N. For this reason in this paper we do not rely upon neutron data but always estimate the Néel temperature from x-ray and resistivity data.

A qualitative magnetic phase diagram for the Cr(2000 Å)/V heterostructure as derived from neutron and synchrotron scattering experiments is shown in Fig. 5. The

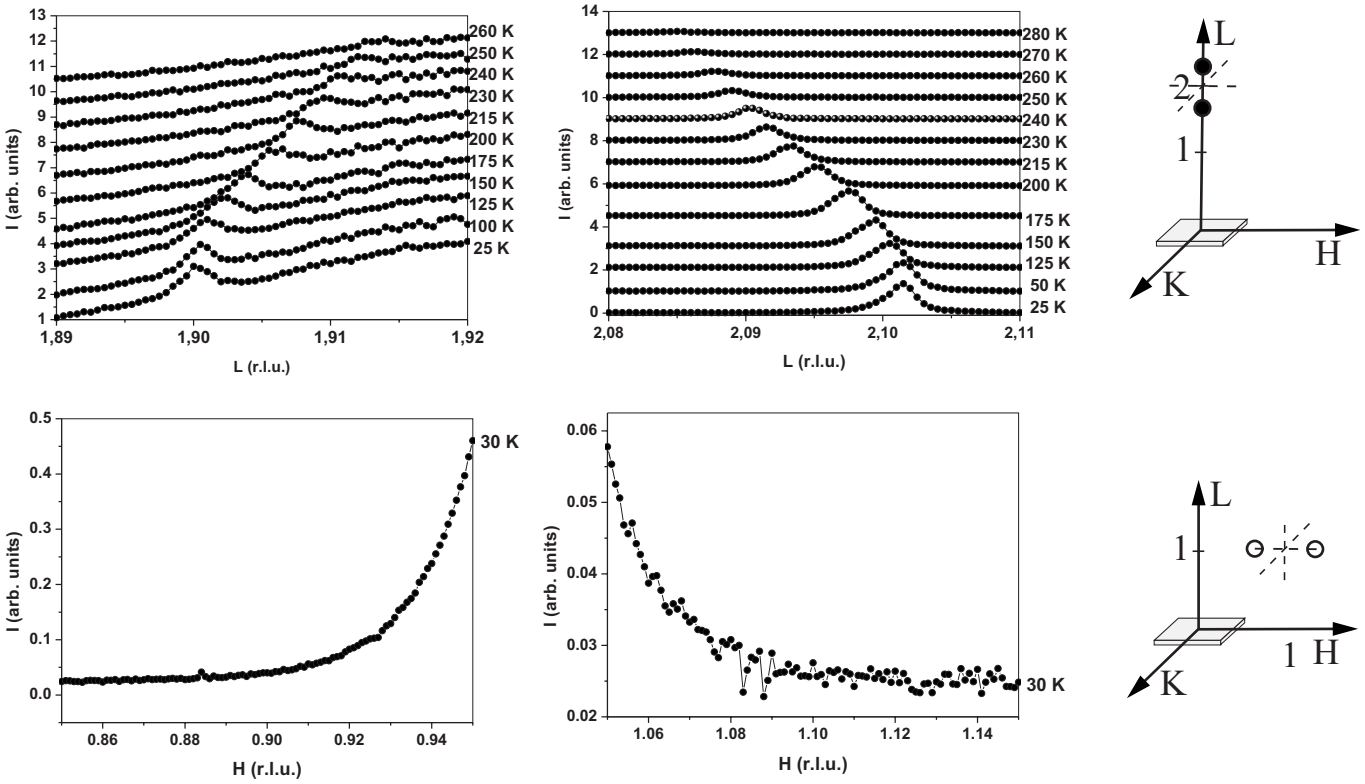

FIG. 3. Synchrotron radiation scans from the Cr(2000 Å)/V sample measured along the L direction around the Cr(002) reflection and along the H direction around the Cr(101) peak. The fundamental (002) and (101) Cr peaks are removed from the figures since their intensities are many orders of magnitude higher than the intensities of the satellite reflections. The individual scans taken at different temperatures are shifted vertically by a constant factor for clarity.

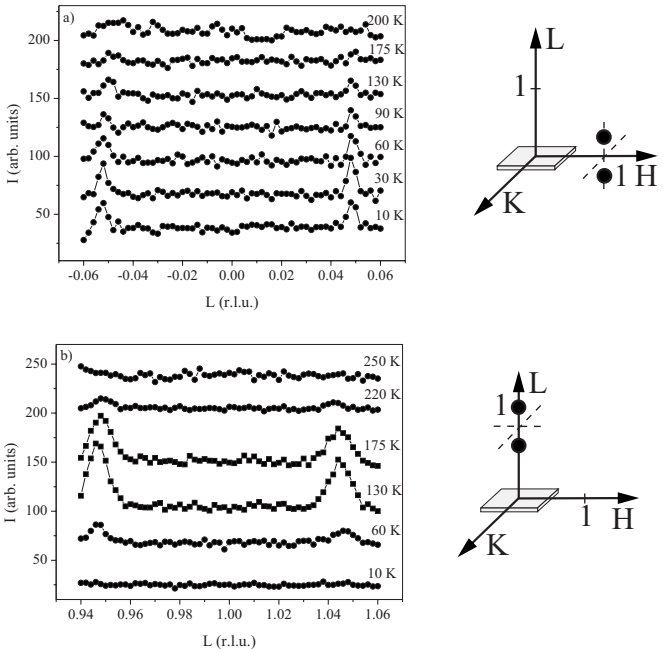

FIG. 4. Neutron scattering scans from the sample Cr(2000 Å)/V taken in the *L* direction around the Cr(100) and the Cr(001) positions to explore the SDW polarization. The scans recorded at different temperatures are depicted with an offset in the vertical direction for clarity. Scans performed in the *K* direction around these positions detected no scattered intensity.

SDW in the heterostructure propagates always in the out-of-plane direction; it has longitudinal polarization at low temperatures and transverse polarization at higher temperatures. For the temperatures $T > T_N$ the system becomes completely paramagnetic and there exists no SDW anymore. No commensurate SDW was detected in the sample. This magnetic phase diagram is very similar to that of bulk Cr, with the only difference being slightly lower spin-flip and Néel temperatures. The decrease in these characteristic temperatures is well known as a rather common property of Cr thin-films.

(ii) $[\mathrm{Cr}(1000\ \text{Å})/\mathrm{V}]_2$ *heterostructures*. As was discussed above, we detected two structural phases for the Cr(1000 Å)/V sample. It is reasonable to expect that these phases would also provide two different types of SDWs. In Fig. 6 are presented synchrotron radiation scans from the Cr(1000 Å)/V heterostructure taken at different temperatures. As evident from the picture, in this case we observe SW satellites arising in the *L* direction around the Cr(002) fundamental Bragg reflection as well as those in the *H* direction around the Cr(101) fundamental Bragg reflection. The first set of satellites is associated with out-of-plane SWs and the second one with in-plane waves. The in-plane and out-of-plane phases have different Néel temperatures as well as different wave periods. The ratio of the integral intensities of the in-plane and out-of-plane SW satellite reflections is about 1:10. This corresponds well to the ratio of relative volumes occupied by different crystallographic phases as estimated from x-ray structural investigations (see Sec. II), taking into account the difference in structure factors for the SW satellite reflections near (002) and (101) Cr fundamental Bragg reflections. Thus, we can identify the in-plane SWs with the minor crystallographic phase in this sample and the out-of-plane SWs with the major phase. The difference between these two phases is due to a significant difference in the in-plane lattice parameters; i.e., there is a significant difference in the in-plane tensile epitaxial strain applied to these two phases. We conclude that generally SWs propagate out of plane in this heterostructure but in the presence of in-plane epitaxial tensile strain it is possible to cause a reorientation of the SW to the in-plane propagation direction.

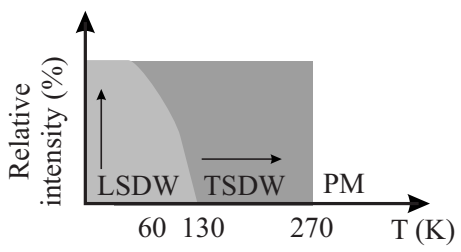

FIG. 5. Qualitative magnetic phase diagram for the spin-density waves in the Cr(2000 Å)/V heterostructure. The phase diagram is the result of combined synchrotron and neutron scattering experiments, as described in the text. The arrows indicate the orientation of the Cr magnetic moments relative to the horizontal Cr film.

The SDW polarization in the multilayer was confirmed again by neutron diffraction. The in-plane SDW was found to be very difficult to measure due to low scattered intensity. In the time available we were able to carry out only one screening scan at 2 K in the *H* direction around the (100) and (001) Cr positions and we have found that the in-plane SDW is a transverse SDW with out-of-plane spins. The out-of-plane SDW was investigated in more detail. In Fig. 7 is shown the neutron scan taken in the *L* direction around the Cr (100) position. The scan done in the *L* direction around the Cr(001) position detected no scattered intensity, and we do not present it here. As is evident from Fig. 7, there is no spin-flip transition and the out-of-plane SDW is a longitudinal wave at all temperatures up to 270 K where it becomes a commensurate SDW. The Néel temperature for the incommensurate phase of 270 K is estimated from the synchrotron scattering data. The transition from the incommensurate phase to the commensurate phase is not sharp but spread over a temperature interval from 250 K to 270 K. We were not able reach the Néel temperature for the commensurate phase, and we just suppose that it can be well above room temperature. It is important to note that the SDW polarization with out-of-plane spins does not change during the phase transition from the incommensurate SDW to the commensurate SDW, so the phase transition is only characterized by a change in the value of Cr magnetic moments.

A qualitative magnetic phase diagram for the Cr(1000 Å)/V heterostructure is shown in Fig. 8 as it was deduced from the neutron and synchrotron scattering data. At low temperatures there exist two incommensurate SDWs: an out-of-plane longitudinal SDW and an in-plane transverse one with out-of-plane spins. The in-plane and out-of-plane SDWs have different Néel temperature as shown in the phase diagram. The out-of-plane SDW becomes a commensurate SDW at temperatures above 250 K, and it exists in the multilayer well above room temperature. No conclusion can

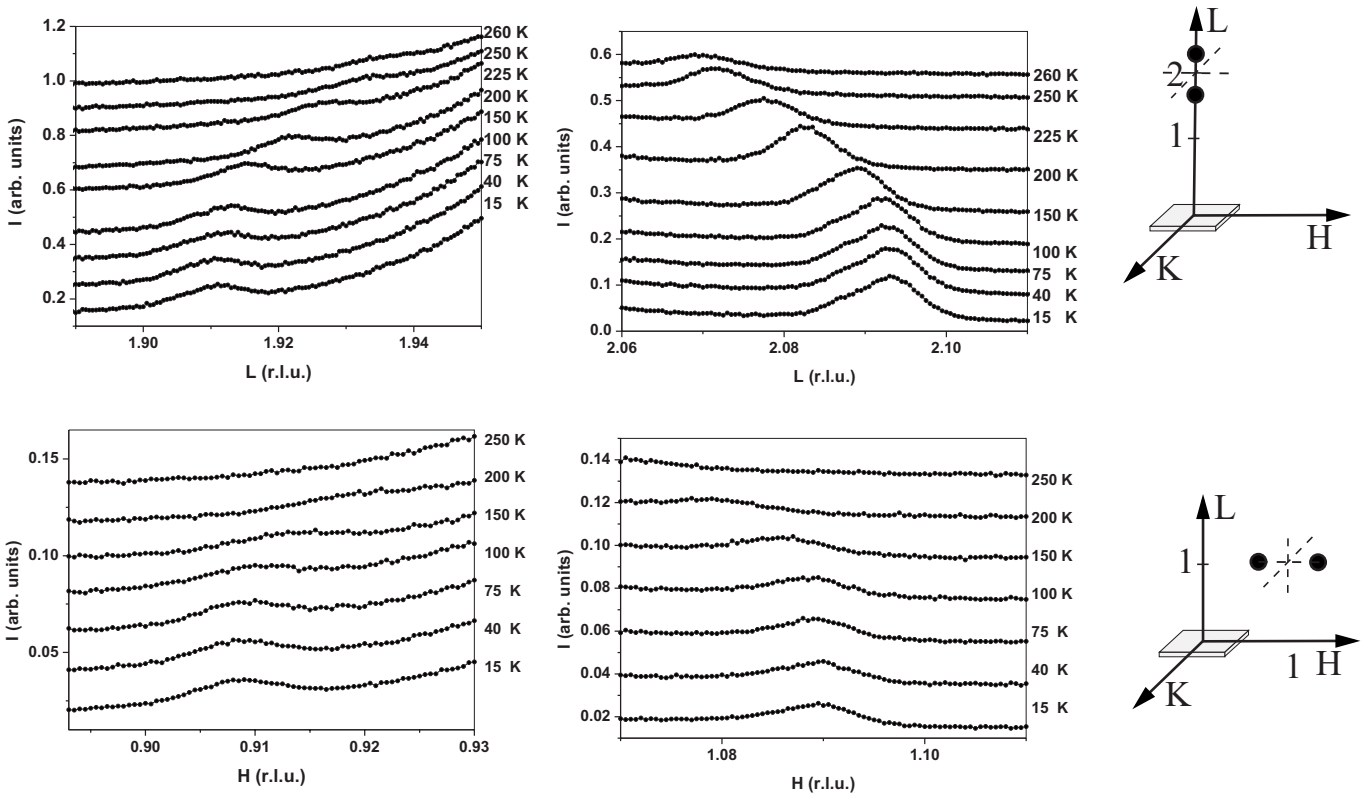

FIG. 6. Synchrotron radiation scans from the Cr(1000 Å)/V sample measured along the L direction around the Cr(002) reflection and along the H direction around the Cr(101) peak. The fundamental (002) and (101) Cr peaks are again removed from the figures since their intensities are many orders of magnitude higher than the intensities of the satellite reflections. The individual scans taken at different temperatures are shifted vertically by a constant factor for clarity.

be drawn concerning the behavior of the in-plane SDW at higher temperatures. We can only note that, to the best of our knowledge, up to now no evidence has been found for a spin-flip transition from transverse to longitudinal incommensurate SDWs with increasing temperature. There may be only a transition from a transverse incommensurate SDW to a commensurate SDW or to a paramagnetic phase. The existence of a transverse SDW in Cr films at very low temperatures was only reported by Kunnen *et al.*[21] for a Cr(001) films grown directly onto MgO(001) substrates, with a very strong in-plane tensile strain.

(iii) $[\mathrm{Cr}(500\ \text{Å})/\mathrm{V}]_4$ *heterostructures*. Next we present results for the SDW state in the Cr(500 Å)/V heterostructure. In this case the SDW behavior was found to be much simpler compared to the above two heterostructures. In Fig. 9 are presented synchrotron radiation scans from the Cr(500 Å)/V heterostructure taken at different temperatures. As evident from the scans, the SW propagates only in the out-of-plane direction and no in-plane phase was detected. In Fig. 10 is shown the neutron scan taken in the L direction around the

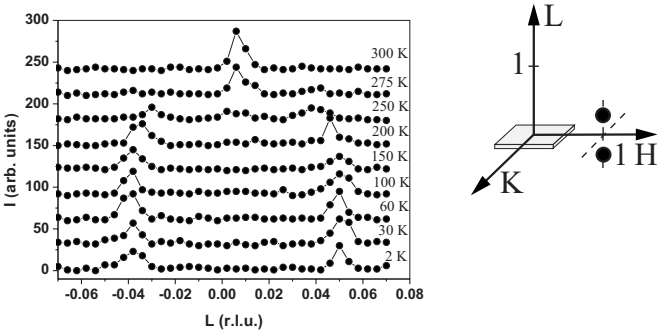

FIG. 7. Neutron scattering scans from the sample Cr(1000 Å)/V taken in the L direction around the Cr(100) position to explore the SDW polarization. The scans recorded at different temperatures are depicted with an offset in the vertical direction for clarity. No scattered intensity was detected in the L direction around the Cr(001) position and we do not show this scan here.

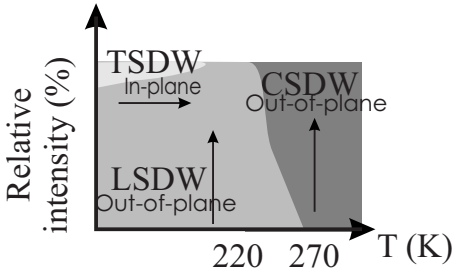

FIG. 8. Qualitative magnetic phase diagram for the spin-density wave in the Cr(1000 Å)/V heterostructure. The phase diagram is the result of combined synchrotron and neutron scattering experiments, as described in the text. The arrows indicate the orientation of the magnetic moments. The small text labels "in-plane" and "out-of-plane" refer to the propagation directions of the SDWs.

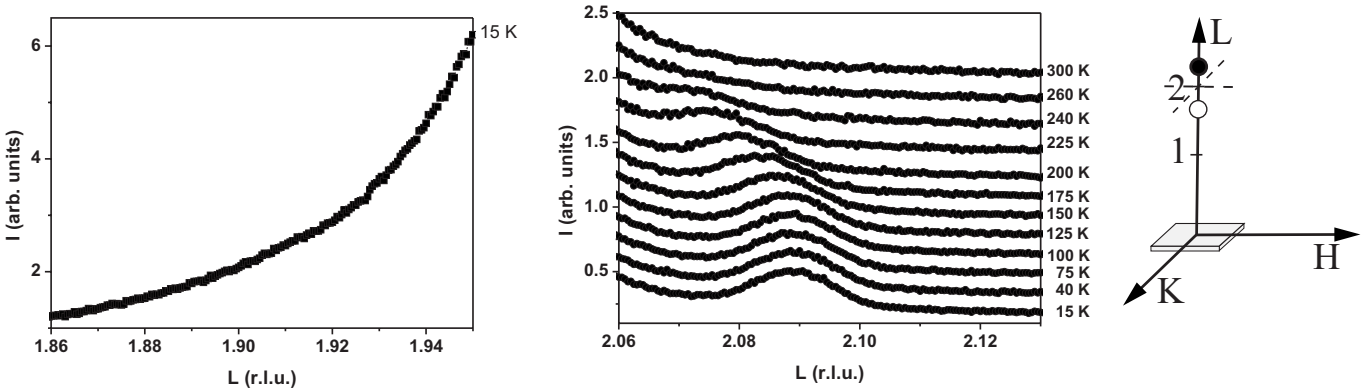

FIG. 9. Synchrotron radiation scans from the Cr(500 Å)/V sample measured along the *L* direction around the Cr(002) reflection. The fundamental (002) Cr Bragg peak is again removed from the figures since its intensity is many orders of magnitude higher than the intensities of the satellite reflections. No satellites are visible in the scan made on the left-hand side of the (002) position due to strong contamination from the very broad V(002) reflection. The individual scans taken at different temperatures are shifted vertically by a constant factor for clarity.

Cr (100) position. The other three scans detected no scattered intensity, and they are not presented here. As follows from the neutron data of Fig. 10, the SDW is a longitudinal incommensurate SDW at low temperatures and it becomes a commensurate SDW at temperatures above 250 K. The transition from the incommensurate phase to the commensurate one is again not sharp, and both waves coexist in the temperature interval from 220 to 250 K. A qualitative magnetic phase diagram for the Cr(500 Å)/V multilayer is shown in Fig. 11.

(iv) $[Cr(250\ Å)/V]_8$ *heterostructures*. In Fig. 12 are shown synchrotron radiation scans from the Cr(250 Å)/V heterostructure measured at different temperatures. Again, as follows from Fig. 12, in this case the strain wave propagates entirely out of the film plane, whereas the in-plane wave is completely suppressed. The Néel temperature for the incommensurate phase is now estimated to be about 150 K—i.e., much lower than found for the samples discussed above. It is important to note that the SW satellite peak position is temperature independent, implying that the SDW period is also temperature independent for this sample.

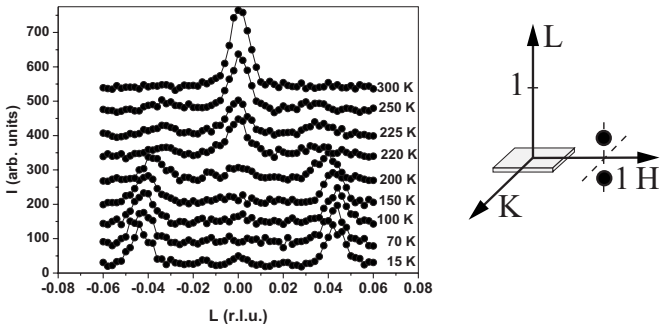

FIG. 10. Neutron scattering scans from the sample Cr(500 Å)/V taken in the *L* direction around the Cr(100) position to explore the SDW polarization. The scans recorded at different temperatures are depicted with an offset in the vertical direction for clarity. No scattered intensity was detected in the *L* direction around the Cr(001) position and in the *K* direction around the Cr(100) and Cr(001) positions; therefore, these scans are not presented.

The magnetic phase diagram is determined from the neutron scattering experiment. Again, we have detected the scattered intensity only in the *L* direction around the Cr(100) positions. This scan is presented in Fig. 13. As follows from the neutron scattering data, in this sample there coexist both an incommensurate longitudinal SDW and a commensurate phase staying from very low temperatures. No spin-flip transition was observed for the incommensurate SDW, and it stays longitudinal up to the Néel temperature of 150 K. The volume occupied by the incommensurate phase decreases with temperature and, conversely, the commensurate phase expands with temperature. Both SDW phases have the same polarization with the Cr magnetic moments being oriented out-of-plane. At temperatures above 150 K only the commensurate SDW persists and it stays well above room temperature. A qualitative magnetic phase diagram for the Cr(250 Å)/V multilayer is shown in Fig. 14.

(v) $[Cr(125\ Å)/V]_{16}$ *heterostructures*. Next we consider a Cr(125 Å)/V multilayer. No scattered SW signal was detected in the superlattice with synchrotron radiation, which implies that there is no incommensurate SDW within the sample. This conclusion is supported by neutron scattering

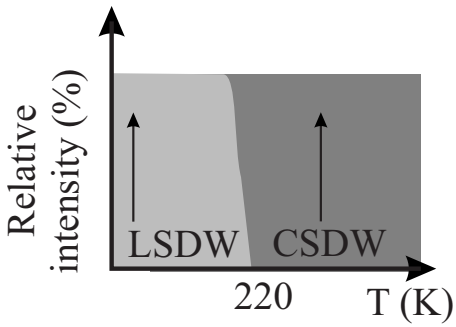

FIG. 11. Qualitative magnetic phase diagram for the spin-density wave in the Cr(500 Å)/V heterostructure. The phase diagram is the result of combined synchrotron and neutron scattering experiments, as described in the text. The arrows indicate the orientation of the Cr magnetic moments relative to the horizontal Cr layers.

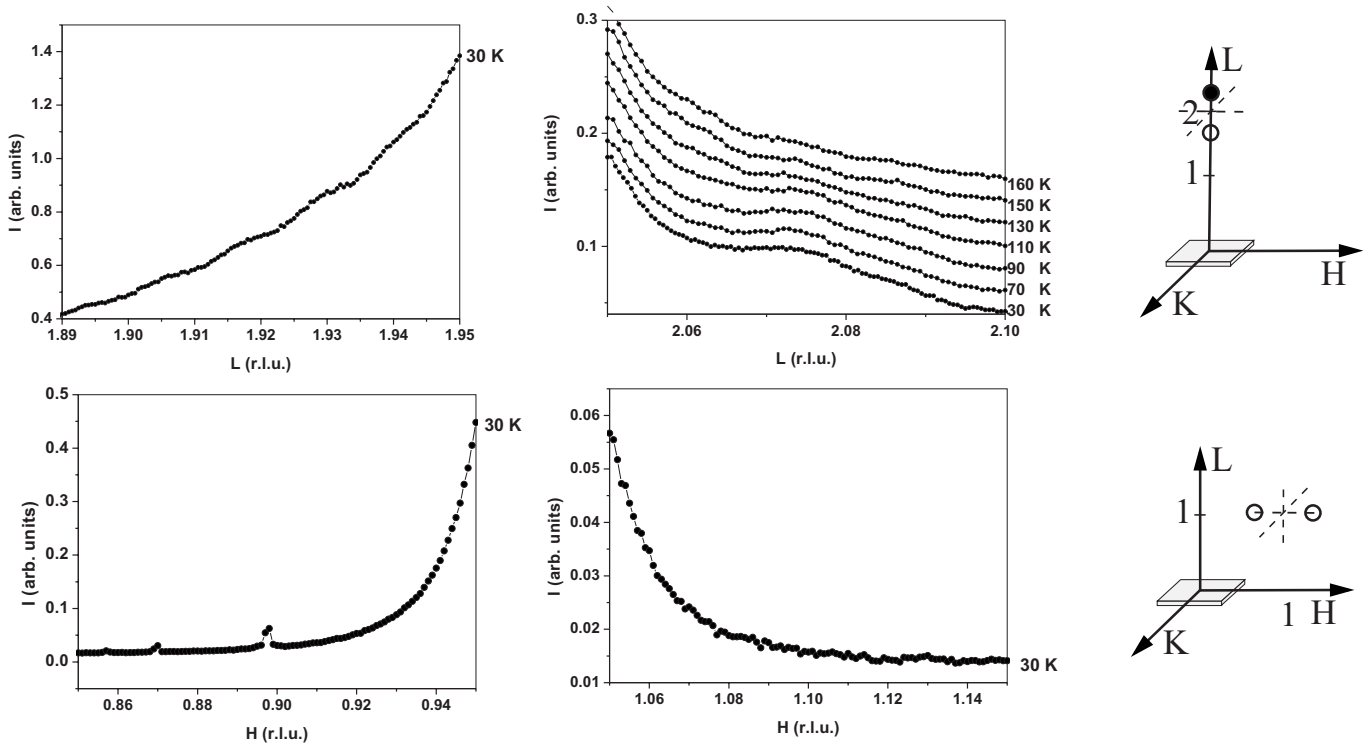

FIG. 12. Synchrotron radiation scans from the Cr(250 Å)/V sample measured along the *L* direction around the Cr(002) reflection and along the *H* direction around the Cr(101) peak. The fundamental (002) and (101) Cr peaks are again removed from the figures since their intensities are many orders of magnitude higher than the intensities of the satellite reflections. The individual scans taken at different temperatures are shifted vertically by a constant factor for clarity. Small peaks at the left bottom picture are due to contaminations not related to strain waves.

results presented in Fig. 15. As follows from the picture, the sample is completely occupied by a commensurate SDW with out-of-plane magnetic moments, with magnetic moments changing in the out-of-plane direction. The commensurate phase exists from the lowest temperatures to well above the room temperature. A magnetic phase diagram for the Cr(125 Å)/V superlattice is depicted in Fig. 16.

(vi) $[Cr(90\ Å)/V]_{23}$ *superlattice*. Finally we consider a Cr(90 Å)/V multilayer. The sample was measured both with synchrotron radiation and with neutron scattering but in neither case were peaks related to SWs or SDWs detected. In Fig. 17 are presented neutron scattering scans taken in the *L* direction around the (100) and (001) Cr positions that show no peaks. Scans taken around these positions in the *H* direction have also not shown any peaks. So we conclude that the Cr(90 Å)/V superlattice is paramagnetic at all temperatures.

VI. DISCUSSION

As discussed in the Introduction, analysis of the SDW behavior in Cr-based multilayers is often complicated by the

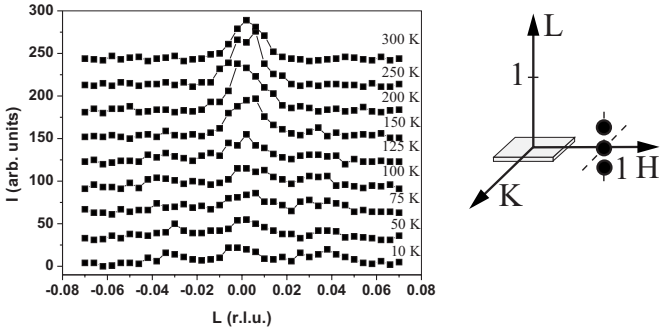

FIG. 13. Neutron scattering scans from the sample Cr(250 Å)/V taken in the *L* direction around the Cr(100) position to explore the SDW polarization. The scans recorded at different temperatures are depicted with an offset in the vertical direction for clarity. No scattered intensity was detected in the *L* direction around the Cr(001) position; we do not show this scan here.

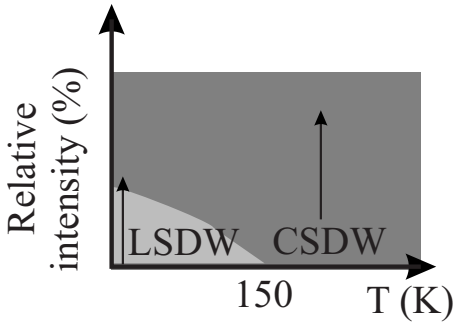

FIG. 14. Qualitative magnetic phase diagram for the spin-density wave in the Cr(250 Å)/V heterostructure. The phase diagram is the result of combined synchrotron and neutron scattering experiments, as described in the text. The arrows indicate the orientation of the Cr magnetic moments relative to the horizontal Cr layers.

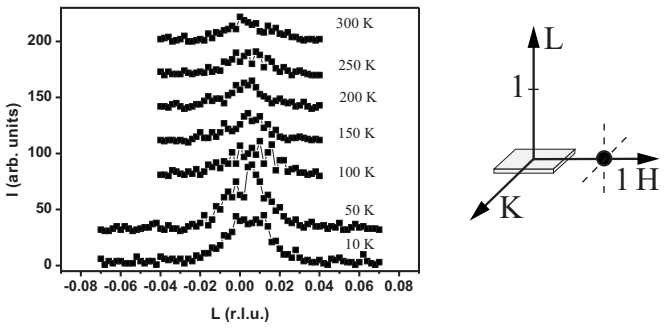

FIG. 15. Neutron scattering scans from the sample Cr(125 Å)/V taken in the *L* direction around the Cr(100) position to explore the SDW polarization. The scans recorded at different temperatures are depicted with an offset in the vertical direction for clarity. No scattered intensity was detected in the *L* direction around the Cr(001) position; we do not show this scan here.

fact that many competitive factors may play their parts in forming the SDW state. In order to work out essential details, we estimate first the relative importances of these factors in our case of Cr/V heterostructures. As follows from our structural analysis, the samples of the series have a high degree of structural coherence. Epitaxial strains due to the Cr-V and Cr-MgO lattice misfits are not so essential and do not change significantly with Cr thickness. In fact, the strongest strain is in the thickest Cr layers and it weakens with decreasing Cr thickness. The only exception is the minor in-plane phase observed in the Cr(1000 Å)/V sample. Comparison of the in-plane and out-of-plane phases in this sample gives us a chance to identify the role of in-plane epitaxial tensile stress in the SDW behavior, which we will discuss below in some detail. The crystal coherence becomes worse at small Cr thicknesses but it is high enough that it should not limit SDWs. So when considering the main SDW phases we can exclude from our analysis effects related to epitaxial strains and structural imperfections, which are sometimes considered important in Cr thin films based on known observations for bulk Cr.[25]

Our structural data also provide clear experimental evidence for a good layer structure and well-defined interfaces

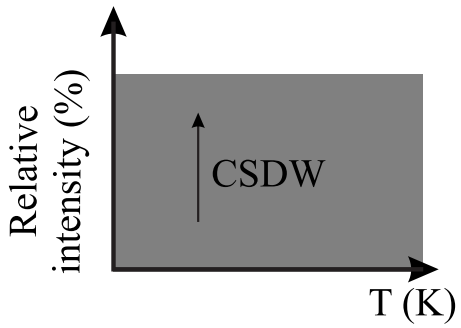

FIG. 16. Qualitative magnetic phase diagram for the spin density wave in the Cr(125 Å)/V heterostructure. The phase diagram is the result of combined synchrotron and neutron scattering experiments, as described in the text. The arrows indicate the orientation of the Cr magnetic moments relative to the horizontal Cr layers. No incommensurate SDW exists in the sample, and it is completely occupied by the commensurate phase from the lowest temperature.

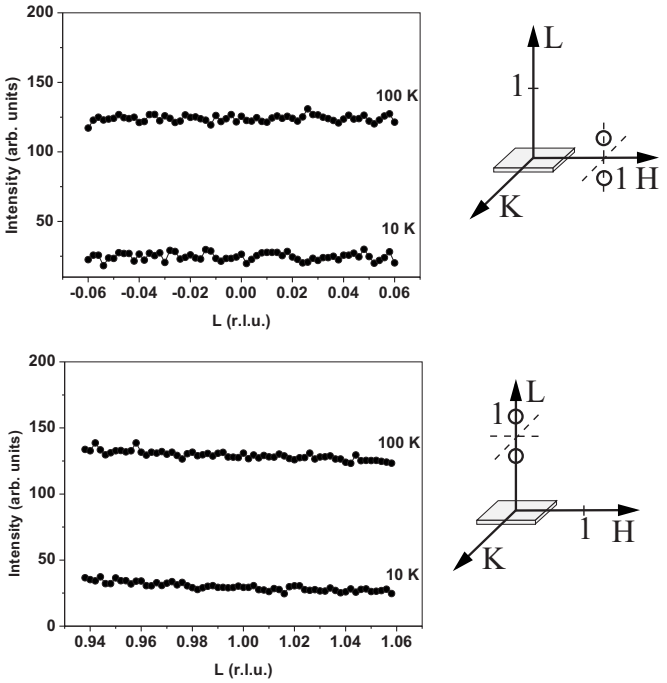

FIG. 17. Neutron scattering scans from the sample Cr(90 Å)/V taken in the *L* direction around the Cr(100) and (001) positions to seek the SDW polarization. Similarly, no scattered intensity was detected in the *H* direction around the (001) and (100) Cr positions; we do not show these scans here.

in the samples under consideration. The observed interface roughness of a few angstroms is much less than the thickness of the magnetically interfacial dead region near Cr/V interfaces, which occupies from 10–20 Å (Ref. 17) to 50 Å (our estimate discussed below). Since the influence of the interface imperfectness should be screened out at such distances, we do not expect the Cr/V interface properties to play an important part in the formation of the SDW state. This conclusion is also in line with results of Ref. 17 where it was reported that Cr magnetic moments in Cr/V multilayers do not depend on growth conditions.

We will focus our attention mainly on the three main factors responsible for the SDW properties in our Cr/V heterostructures: (i) the spontaneous formation of the SDW in Cr due to the Fermi surface nesting, (ii) finite-size effects (Cr thickness dependence), and (iii) proximity effects from neighboring V layers, which include, in particular, Cr-V interface hybridization, possible formation of magnetically dead regions near Cr/V interfaces, and specific electronic boundary conditions for SDWs at Cr/V interfaces.

The synchrotron and neutron scattering data discussed above provide a clear and systematic picture of the SDW magnetism in Cr/V multilayers. The onset of a bulklike SDW state in Cr/V comes through several steps from a paramagnetic state in thinnest Cr layers to a commensurate SDW in thicker ones and finally to an incommensurate SDW in the thickest layers. It is already reported[17] that there is a magnetically dead Cr region near Cr/V interfaces, so Cr/V multilayers are expected to be nonmagnetic for thin enough Cr layers. We have found the Cr(t_{Cr})/V(14 Å) multilayers are nonmagnetic for Cr thicknesses t_{Cr} up to at least 90 Å. Next,

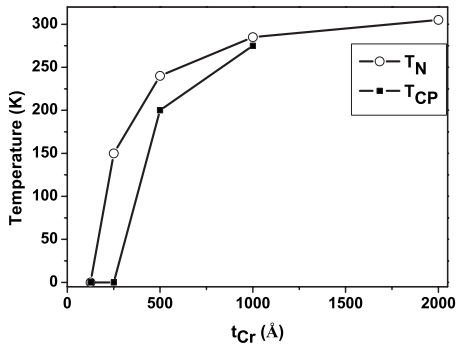

FIG. 18. Néel temperature of the incommensurate SDW, T_N, and the temperature of the commensurate SDW appearing T_{CP} as functions of Cr layer thickness in the Cr/V heterostructures. We note that both of them scale with Cr thickness. The solid lines connecting the data points are guides for the eyes.

at a Cr thickness between 90 and 125 Å the Cr magnetism suddenly appears in the form of a commensurate SDW. As we discuss below, the thickness of a magnetically dead layer near Cr/V interfaces would be about 50 Å; i.e., the critical thickness for CSDW to appear is expected to be about 100 Å. The Néel temperature for the commensurate phase seems to be well above room temperature. As the Cr thickness increases further, an incommensurate SDW phase starts to occur at low temperatures where it coexists with the commensurate SDW phase. We observed a low-temperature incommensurate SDW in the samples with $t_{Cr} \geqslant 250$ Å. As Cr layers become thicker, the Néel temperature T_N for the incommensurate SDW increases and the commensurate SDW occurs at higher temperatures close to T_N. In the case of very thick Cr layers of about 2000 Å we observe only the incommensurate SDW.

The Néel temperature T_N for the incommensurate SDW phase scales with the Cr thickness approaching a bulklike value for thick Cr films of about 2000 Å. The temperature T_{CP} at which the commensurate phase starts to appear also scales with Cr thickness approaching T_N. In the sample with $t_{Cr}=2000$ Å, the commensurate SDW phase does not occur at all and the SDW behavior becomes very similar to that in bulk Cr. In Fig. 18 are shown T_N and T_{CP} as functions of Cr layer thickness. We note that the scaling behavior for $T_N(t_{Cr})$ in Cr/V multilayers is drastically different from that reported for Cr/Fe.[9] According to Fullerton *et al.*,[9] the incommensurate phase in Cr/Fe appears at $t_{Cr}=48$ Å; T_N increases rapidly with Cr thickness and reaches a bulklike value at $t_{Cr}=200$ Å. In Cr/V multilayers, the incommensurate SDW starts to appear only in much thicker Cr layers with t_{Cr} between 125 and 250 Å and T_N reaches a bulklike value at a Cr thickness of about 2000 Å.

The temperature dependence of the ISDW period in Cr/V was found to depend significantly on the Cr thickness. The data deduced from synchrotron measurements are plotted in Fig. 19 and compared to the SDW period in bulk Cr (Ref. 26) and bulk $Cr_{0.995}V_{0.005}$ alloy.[27] The SDW period in Cr/V does not follow the temperature dependence observed in CrV alloys and appears to be more similar to results reported for thin Cr films,[3] where it is enhanced compared to bulk Cr and scales inversely with the Cr thickness. The exception is the

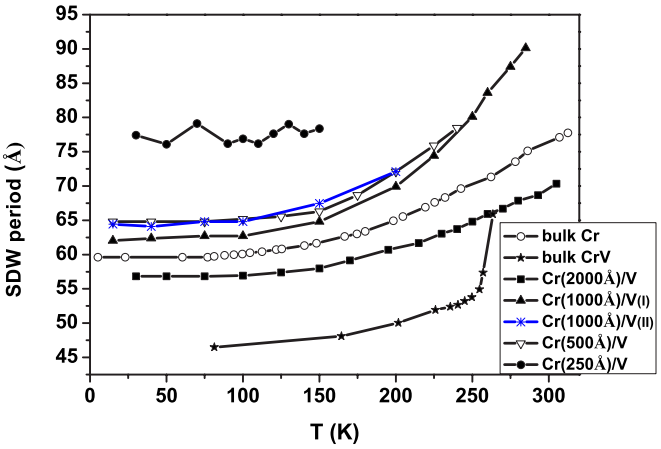

FIG. 19. (Color online) Temperature dependence of the incommensurate spin-density-wave period in the Cr/V heterostructures as revealed from our synchrotron measurements and corresponding data for reference systems: bulk Cr (Ref. 26) and bulk $Cr_{0.995}V_{0.005}$ alloy (Ref. 27). For the Cr(1000 Å)/V sample we show two phases: the major (out-of-plane) phase I occupying 95% of the sample and the minor (in-plane) phase II occupying the remaining 5%. The solid lines connecting the data points are guides for the eyes.

Cr(2000 Å)/V sample where the SDW period is smaller than in bulk Cr, which is highly atypical for thin Cr films. It could be that the Cr-V proximity effect favors decreasing the SDW period in contrast to the finite-size effect. In addition to these finite-size effects known also for other systems, we note an important feature that seems to be characteristic of Cr/V and has not been reported yet in other systems. As discussed above, the SDW is strictly confined in Cr/V and forced to have nodes at Cr/V interfaces; i.e., it always must include an integer number of half periods. The actual value of the SDW period may be enhanced or decreased in order to fit an integer number of half periods to the space provided. Any change of the SDW period with temperature should follow the corresponding change in the number of half periods or in the space occupied. If the space does not change, the SDW period should be independent of temperature as we observe in the Cr(250 Å)/V sample. However, the Cr(500 Å)/V sample shows a strong temperature dependence of the SDW period. To understand this dependence, we have to assume that the number of SDW nodes decreases. By decreasing the number of half periods from 12 to 10 one should observe jumps in the SDW period.

Another important SDW feature in Cr/V is a strong impact of electronic boundary conditions on the SDW polarization and propagation direction. Both commensurate and incommensurate SDWs in Cr/V are in a similar single-domain state with the magnetic moment modulation in the out-of-plane direction. If the Cr layers are not thick enough, we observe a complete suppression of the spin-flip transition and a stabilization of a longitudinal out-of-plane SDW with out-of-plane spins. Only in the Cr(2000 Å)/V sample with the thickest Cr layers is the spin-flip transition allowed and a transverse SDW propagates in the out-of-plane direction at higher temperatures. Such a stabilization of single-domain out-of-plane SDWs and suppression of the spin-flip transi-

tion are known also for other systems. For example, stabilization of single-domain longitudinal SDWs in Cr/Ag multilayers[28] and transverse ones in Fe/Cr multilayers[10,29] has been reported on. This stabilization phenomenon is often thought to be associated with strains and imperfections in the sample.[28,29] However, our structural investigations do not support this explanation. Alternatively we suggest that the stabilization is due to the influence of the electronic boundary conditions. This influence turns out to be of rather long range and decreases at very large distances of about 2000 Å.

We have given direct experimental evidence for complete suppression of Cr magnetism in Cr/V heterostructures for Cr thickness less than 90 Å. This result was expected because the existence of magnetically dead Cr layers near Cr/V interfaces, which were already theoretically predicted by Hirai[16] and experimentally observed with Mössbauer spectroscopy by Almokhtar *et al.*[17] In Ref. 17 it was reported that such a suppression occurs in Cr(80 Å)/V(10 Å) superlattices at distances of about 10–20 Å from Cr/V interfaces, whereas Cr magnetism is restored at distances of more than 20 Å. Our results, however, clearly show that Cr(90 Å)/V(14 Å) superlattices are nonmagnetic. Based on our scattering results we can estimate the thickness of the magnetically dead region in the following way. We have detected no SDW in Cr(90 Å)/V superlattices and a commensurate SDW in Cr(125 Å)/V. This means that the magnetically dead region near Cr/V interfaces should be from 45 to 62 Å in thickness. On the other hand, in the Cr(250 Å)/V sample, an incommensurate phase with a SDW period of 77 Å occurs at low temperatures coexisting with the commensurate SDW phase. Assuming that the incommensurate SDW occupies two periods, we estimate the magnetically dead region to be about 50 Å in thickness. Despite regions of the Cr layers being magnetically dead, coherence of the SDW is maintained across these regions and the V layers in the multilayers as indicated by the magnetic reflections being nearly resolution limited even for thin Cr layers.

We suggest the following explanation for the difference between our data and the results of Ref. 17. Almokhtar *et al.* have probed the magnetic state of Cr by placing a 2-Å-thick ^{119}Sn probe layer in Cr(80 Å)/V(10 Å) superlattices at different distances from the Cr/V interfaces and by measuring the hyperfine field at ^{119}Sn atoms. Further structural x-ray investigations done at Cr/Sn multilayers[30,31] have revealed a nonideal interface structure in these superlattices. It was reported that the rms roughness at Cr/Sn(2 Å) interfaces can exceed several times the nominal Sn thickness, so the probe ^{119}Sn layers may be considered as impurities or defects incorporated in Cr layer. In this situation there may occur local Cr magnetic moments due to the formation of local spin-density waves in the vicinity of Cr/Sn interfaces. Such local spin-density waves have been observed in a number of Cr alloys,[2] in particular above the Néel temperature in CrV alloys, where they are explained by stabilization of a short-range order around impurities and defects.[32] Enhanced Cr magnetic fields at Cr/Sn interfaces were also reported to be detected by Mössbauer spectroscopy.[33,34] We speculate that Almokhtar *et al.*[17] may have detected local Cr magnetic moments that appeared due to nonideal structures and local strains at Cr/Sn interfaces in Cr/V superlattices, which would be nonmagnetic without Sn probe layers. The 50-Å dead-layer thickness agrees well with the proximity effects observed in V/Cr/Fe heterostructures, where for a thickness of 50 Å a strong suppression of T_c was observed.[35]

Next we discuss the coexistence and competition between commensurate and incommensurate SDW phases in Cr/V. Commensurate SDWs are often reported in Cr thin films[3] and are generally thought to be associated with sample imperfections or epitaxial strains in analogy with bulk Cr.[1] In particular, Fritzsche *et al.*[36] reported the total suppression of incommensurate SDWs and domination of commensurate ones in (110)Cr(300 Å)/V(50 Å) multilayers, relating it to strains and structural imperfections.

We found that, for sufficiently thin Cr films, magnetic order in Cr/V multilayers may only exist as a commensurate SDW. Similar SDW behavior is also known for Cr/Fe multilayers[10,11] where only a commensurate SDW was detected for Cr thicknesses less than a critical value about 50 Å. It was theoretically explained[37] that an incommensurate SDW cannot develop until the structural correlation length (film thickness in this case) is more than one period of the spin-density wave. The same explanation can be directly applied to the Cr(125 Å)/V sample if one takes into account the existence of magnetically dead regions of about 50 Å in thickness at both sides of the C layer the near Cr/V interfaces.

Reviewing the phase diagrams for the samples with thicker Cr layers, the above explanations may be not enough to understand them. In the Cr(250 Å)/V sample, for instance, the Cr thickness is thick enough for an incommensurate SDW to develop and it does occur. But we also observe a commensurate SDW, which coexists with the incommensurate SDW at low temperatures and persists up to high temperatures. Since the incommensurate SDW period does not change with temperature, the boundary between the commensurate and incommensurate SDW phases may not move in the out-of-plane direction but only in the in-plane direction. The Cr layers are likely to be occupied by both ISDW and CSDW phases separated by out-of-plane boundaries. The CSDW phase is not localized near Cr/V interfaces but distributed uniformly in the out-of-plane direction. As the Cr layers become thicker the commensurate SDW occurs at higher temperatures and the characteristic temperature T_{CP} scales with Cr thickness approaching the Néel temperature for the incommensurate SDW.

As already mentioned, the occurrence of commensurate SDWs at elevated temperatures is often reported in Cr thin films[22,38] and is generally associated with sample imperfections, epitaxial strains, or interface effects. In our view, these common explanations cannot be applied to our Cr/V heterostructures. As we discussed above, structural and strain arguments cannot be applied to this case. We do not see a correlation between the sample structure and the CSDW properties. Since the commensurate SDW is not located near interfaces, we have also to exclude interface effects. On the other hand, commensurate SDW properties are definitely affected by finite-size and proximity effects. We believe that the CSDW polarization and propagation are completely determined by electronic boundary conditions, as well as the Cr

thickness, which affects the characteristic temperature T_{CP}. The CSDW disappears completely in the Cr(2000 Å)/V sample, where the influence of boundary conditions becomes weaker and the system approaches bulklike behavior without the stabilization of a longitudinal SDW. In our view, the origin of commensurate SDWs in the Cr/V system should be reexamined by theoreticians.

Finally, we briefly discuss the influence of epitaxial strains on the SDW behavior in Cr/V. As we know, the main SDW phases in our Cr/V samples are not strongly affected by epitaxial strains. Fortunately, we have a chance to show this influence by analyzing the properties of the minor phase II in the Cr(1000 Å)/V which is highly affected by in-plane tensile strains. The main phase I in this sample is characterized by a longitudinal SDW out-of-plane propagation, and the spin-flip transition is completely suppressed. Strong in-plane tensile strain causes an SDW reorientation (minor phase II) from the out-of-plane to in-plane direction, changes the SDW polarization from longitudinal to transverse, and enhances the SDW period. The Néel temperature for the incommensurate SDW drops from 285 K for the main phase to 220 K for the minor one.

VII. CONCLUSIONS

We have presented a systematic investigation of the thickness dependence of the SDW magnetism in Cr/V heterostructures using a combination of resistivity, neutron, and synchrotron scattering experiments. We have demonstrated that the SDW behavior in Cr/V is strongly affected by Cr Fermi-surface nesting, finite-size effects, and proximity effects from neighboring V layers. Cr magnetism is completely suppressed in Cr/V heterostructures with Cr thickness less than 100 Å. As the Cr thickness increases, the magnetic state in Cr/V changes from a paramagnetic state to a commensurate SDW and finally to an incommensurate SDW in thick Cr layers. The Cr-V proximity effect has a long-range nature and causes stabilization of longitudinal out-of-plane SDWs. The Néel temperature for the incommensurate SDW is found to scale with Cr thickness and reaches a bulklike value at very large Cr thicknesses of about 2000 Å. High-temperature commensurate SDWs persist over a wide interval of Cr thicknesses and disappear completely only in samples with very thick Cr layers of about 2000 Å in thickness.

ACKNOWLEDGMENTS

We would like to thank Oliver Seeck and Christian Sternemann for help with the instrument operation at the W1.1 (HASYLAB) and SAW (DELTA) beamlines. This work was supported by Sonderforschungsbereich 491 "Magnetische Heteroschichten: Struktur und elektronischer Transport" funded by the Deutsche Forschungsgemeinschaft.

*Present address: Advanced Photon Source, Argonne National Laboratory, Argonne, IL 60439, USA.
†Present address: Hahn-Meitner-Institut Berlin GmbH, D-14109, Berlin, Germany.
‡Present address: BESSY GmbH, D-12489, Berlin, Germany.
§Present address: Department Mobility and Environment, EMPA, CH-8600 Dübendorf, Switzerland.

[1] E. Fawcett, Rev. Mod. Phys. **60**, 209 (1988).
[2] E. Fawcett, H. L. Alberts, V. Yu. Galkin, D. R. Noakes, and J. V. Yakhmi, Rev. Mod. Phys. **66**, 25 (1994).
[3] H. Zabel, J. Phys.: Condens. Matter **11**, 9303 (1999).
[4] R. S. Fishman, J. Phys.: Condens. Matter **13**, R235 (2001).
[5] D. T. Pierce, J. Unguris, R. J. Celotta, and M. D. Stiles, J. Magn. Magn. Mater. **200**, 290 (1999).
[6] J. Unguris, R. J. Celotta, and D. T. Pierce, Phys. Rev. Lett. **67**, 140 (1991).
[7] J. Unguris, R. J. Celotta, and D. T. Pierce, Phys. Rev. Lett. **69**, 1125 (1991).
[8] J. Mattson, B. Brumitt, M. B. Brodsky, and J. B. Ketterson, J. Appl. Phys. **67**, 4889 (1990).
[9] E. E. Fullerton, K. T. Riggs, C. H. Sowers, S. D. Bader, and A. Berger, Phys. Rev. Lett. **75**, 330 (1995).
[10] E. E. Fullerton, S. D. Bader, and J. L. Robertson, Phys. Rev. Lett. **77**, 1382 (1996).
[11] A. Schreyer, C. F. Majkrzak, Th. Zeidler, T. Schmitte, P. Bödeker, K. Theis-Bröhl, A. Abromeit, J. A. Dura, and T. Watanabe, Phys. Rev. Lett. **79**, 4914 (1997).
[12] Y. Hamaguchi, E. O. Wollan, and W. C. Koehler, Phys. Rev. **138**, A737 (1965).
[13] W. C. Koehler, R. M. Moon, A. L. Trego, and A. R. Mackintosh, Phys. Rev. **151**, 405 (1966).
[14] A. L. Trego and A. R. Mackintosh, Phys. Rev. **166**, 495 (1968).
[15] S. M. Dubiel, J. Cieslak, and F. E. Wagner, Phys. Rev. B **53**, 268 (1996).
[16] K. Hirai, Phys. Rev. B **66**, 132406 (2002).
[17] M. Almokhtar, K. Mibu, A. Nakanishi, T. Kobayashi, and T. Shinjo, J. Phys.: Condens. Matter **12**, 9247 (2000).
[18] K. Mibu, M. Almokhtar, A. Nakanishi, T. Kobayashi, and T. Shinjo, J. Magn. Magn. Mater. **226-230**, 1785 (2001).
[19] E. Kravtsov, A. Nefedov, F. Radu, A. Remhof, H. Zabel, R. Brucas, B. Hjörvarsson, A. Hoser, and S. B. Wilkins, Phys. Rev. B **70**, 054425 (2004).
[20] E. Kravtsov, A. Nefedov, H. Zabel, R. Brucas, B. Hjörvarsson, A. Hoser, and G. J. McIntyre, J. Phys.: Condens. Matter **17**, 3143 (2005).
[21] E. Kunnen, S. Mangin, V. V. Moshchalkov, Y. Bruynseraede, A. Vantomme, A. Hoser, and K. Temst, Thin Solid Films **414**, 262 (2002).
[22] P. Bödeker, A. Schreyer, and H. Zabel, Phys. Rev. B **59**, 9408 (1999).
[23] J. P. Hill, G. Helgesen, and D. Gibbs, Phys. Rev. B **51**, 10336 (1995).
[24] L. Paolasini, C. Detlefs, C. Mazzoli, S. Wilkins, P. P. Deen, A. Bombardi, N. Kernavanois, F. de Bergevin, F. Yakhou, J. P. Valade, I. Breslavetz, A. Fondacaro, G. Pepellin, and P. BernardJ. Synchrotron Rad. **14**, 301 (2007).

[25] T. J. Bastow and R. Street, Phys. Rev. **141**, 510 (1966).
[26] S. A. Werner, A. Arrott, and H. Kendrick, Phys. Rev. **155**, 528 (1962).
[27] D. R. Noakes, T. M. Holden, P. C. de Camargo, E. Fawcett, and P. de V. DuPlessis, J. Appl. Phys. **64**, 5883 (1988).
[28] M. Rots, S. Demuynck, S. Cottenier, J. Dekoster, and J. Meersschaut, J. Appl. Phys. **85**, 4836 (1999).
[29] S. Demuynck, J. Meersschaut, J. Dekoster, B. Swinnen, R. Moons, A. Vantomme, S. Cottenier, and M. Rots, Phys. Rev. Lett. **81**, 2562 (1998).
[30] A. Gupta, A. Paul, S. Mukhopadhyay, and K. Mibu, J. Appl. Phys. **90**, 1237 (2001).
[31] K. Ishiji, H. Okuda, H. Hashizume, M. Almokhtar, and N. Hosoito, Phys. Rev. B **66**, 014443 (2002).
[32] V. V. Tugushev, in *Modulated and Localized Structures of the Spin-density Wave in Itinerant Antiferromagnets in Electronic Phase Transitions*, edited by W. Hanke and Yu. Kopaev (Elsevier, Amsterdam, 1992), p. 237.
[33] K. Mibu, M. Almokhtar, S. Tanaka, A. Nakanishi, T. Kobayashi, and T. Shinjo, Phys. Rev. Lett. **84**, 2243 (2000).
[34] K. Mibu, M. Takeda, J. Suzuki, A. Nakanishi, T. Kobayashi, Y. Endoh, and T. Shinjo, Phys. Rev. Lett. **89**, 287202 (2002).
[35] M. Hübener, D. A. Tikhonov, I. A. Garifullin, K. Westerholt, and H. Zabel, J. Phys.: Condens. Matter **14**, 8687 (2002).
[36] H. Fritzsche, S. Bonn, J. Hauschild, K. Prokes, and J. Klenke, Eur. Phys. J. B **36**, 175 (2003).
[37] Z. P. Shi and R. S. Fishman, Phys. Rev. Lett. **78**, 1351 (1997).
[38] P. Sonntag, P. Bödeker, A. Schreyer, H. Zabel, K. Hamacher, and H. Kaiser, J. Magn. Magn. Mater. **183**, 5 (1998).